

Unusual thermodynamics of low-energy phonons in the Dirac semimetal Cd_3As_2

Zhen Wang(王振), Hengcan Zhao(赵恒灿), Meng Lyu(吕孟), Junsen Xiang(项俊森), Qingxin Dong(董庆新), Genfu Chen(陈根富), Shuai Zhang(张帅), and Peijie Sun(孙培杰)

Citation: Chin. Phys. B, 2022, 31 (**10**): 106501. DOI: 10.1088/1674-1056/ac8928
Journal homepage: http://cpb.iphy.ac.cn; http://iopscience.iop.org/cpb

What follows is a list of articles you may be interested in

Lattice thermal conductivity of β_{12} and χ_3 borophene

Jia He(何佳), Yulou Ouyang(欧阳宇楼), Cuiqian Yu(俞崔前), Pengfei Jiang(蒋鹏飞), Weijun Ren(任卫君), and Jie Chen(陈杰)

Chin. Phys. B, 2020, 29 (**12**): 126503. DOI: 10.1088/1674-1056/abbbe6

Tuning thermal transport via phonon localization in nanostructures

Dengke Ma(马登科), Xiuling Li(李秀玲), and Lifa Zhang(张力发)

Chin. Phys. B, 2020, 29 (**12**): 126502. DOI: 10.1088/1674-1056/abb7fa

Ultra-low thermal conductivity of roughened silicon nanowires: Role of phonon-surface bond order imperfection scattering

Heng-Yu Yang(杨恒玉), Ya-Li Chen(陈亚利), Wu-Xing Zhou(周五星), Guo-Feng Xie(谢国锋), Ning Xu(徐宁)

Chin. Phys. B, 2020, 29 (**8**): 086502. DOI: 10.1088/1674-1056/ab99af

Effects of surface charges on phonon properties and thermal conductivity in GaN nanofilms

Shu-Sen Yang(杨树森), Yang Hou(侯阳), Lin-Li Zhu(朱林利)

Chin. Phys. B, 2019, 28 (**8**): 086501. DOI: 10.1088/1674-1056/28/8/086501

Anomalous low-temperature heat capacity in antiperovskite compounds

Xin-Ge Guo(郭新格), Jian-Chao Lin(林建超), Peng Tong(童鹏), Shuai Lin(蔺帅), Cheng Yang(杨骋), Wen-Jian Lu(鲁文建), Wen-Hai Song(宋文海), Yu-Ping Sun(孙玉平)

Chin. Phys. B, 2017, 26 (**2**): 026501. DOI: 10.1088/1674-1056/26/2/026501

RAPID COMMUNICATION

Unusual thermodynamics of low-energy phonons in the Dirac semimetal Cd_3As_2

Zhen Wang(王振)[1,2], Hengcan Zhao(赵恒灿)[1], Meng Lyu(吕孟)[1], Junsen Xiang(项俊森)[1], Qingxin Dong(董庆新)[1,2], Genfu Chen(陈根富)[1,2,3], Shuai Zhang(张帅)[1,2,3], and Peijie Sun(孙培杰)[1,2,3,†]

[1] *Beijing National Laboratory for Condensed Matter Physics, Institute of Physics, Chinese Academy of Sciences, Beijing* 100190, *China*
[2] *School of Physical Science, University of Chinese Academy of Sciences, Beijing* 100049, *China*
[3] *Songshan Lake Materials Laboratory, Dongguan* 523808, *China*

(Received 11 May 2022; revised manuscript received 10 June 2022; accepted manuscript online 12 August 2022)

By studying the thermal conductivity, specific heat, elastic modulus, and thermal expansion as a function of temperature for Cd_3As_2, we have unveiled a couple of important thermodynamic features of the low-energy phonons strongly interacting with Dirac electrons. The existence of soft optical phonons, as inferred from the extremely low thermal conductivity, is unambiguously confirmed by low-temperature specific heat revealing significant deviation from Debye's description. The estimated Debye temperature is small in the range of 100–200 K and varies significantly depending upon the measurement used in its experimental determination. The thermodynamic Grüneisen ratio γ reveals a remarkable reduction below about 100 K, an energy scale that is highly relevant to the Dirac states, towards negative values below about 10 K that are indicative of lattice instability.

Keywords: Dirac semimetal, low-energy phonon, thermal conductivity, lattice instability

PACS: 65.40.–b, 65.40.De, 63.20.kd **DOI:** 10.1088/1674-1056/ac8928

1. Introduction

In addition to their electrical and optical properties that have been subjected to intensive investigation, topological semimetals also show intriguing lattice dynamics and thermal properties that remain largely unexplored. Most of these properties concern the interplay between topological electronic bands and low-energy phonons, as highlighted in the following cases: chiral magnetic effect can alter optical phonons via intrinsic plasmon modes in an external magnetic field;[1] topological singularity in electronic bands is able to induce chiral Kohn anomaly in the phonon dispersions;[2] topological phononic and electronic bands in a class of triple-point metals are expected to offer a strategy for enhanced thermoelectricity,[3] etc.

The titled compound Cd_3As_2 is a prototypical Dirac semimetal.[4] It has, on one hand, very high electron mobility derived from symmetry protected Dirac nodes and, on the other hand, surprisingly low lattice thermal conductivity that is indicative of strong phonon scatterings (Refs. [5–8]). The latter phenomenon becomes interesting because of the topological Dirac bands that appear to be highly relevant to lattice dynamics. Thus far, low thermal conductivity has been intensively investigated in thermoelectric materials, most of which host weak chemical bonds that are crucial for reducing phonon velocity and increasing scattering.[9] For Cd_3As_2, a group of soft optical phonons showing Kohn anomaly associated with the Dirac nodes have been identified by *ab initio* calculations.[10] These soft optical modes were ascribed to be the leading reason of the low thermal conductivity by increasing the scattering rate of heat-carrying acoustic phonons. In fact, significant softening of low-energy phonons is generically expected in semimetals near topological phase transition, where Kohn anomalies due to intranode or internode electron–phonon scattering may occur near the Brillouin-zone center.[11] Accordingly, Raman scattering of Cd_3As_2 has shown significant deviations of selected optical-phonon frequencies from the expectation based on lattice anharmonicity below $T \approx 100$ K (Ref. [12]). This has been ascribed to the strong fluctuations of lattice degrees of freedom interacting with Dirac electrons.

From a crystallographic point of view, Cd_3As_2 at ambient conditions crystalizing in the tetragonally distorted antifluorite structure (space group $I4_1/acd$) that hosts topological Dirac bands is located close to a lattice instability. Upon heating to only about 220 °C, it transforms to a Zn_3As_2-type structure with space group ($P4_2/nbc$), with at least two more structural phase transitions taking place at higher temperatures,[13,14] Alternatively, application of pressure causes a couple of structural phase transitions as well, starting from the one at a relatively low pressure of ~ 2.3 GPa.[14–16] Given the complex lattice instability as introduced above, an in-depth investigation on this compound by a comprehensive set of thermodynamic probes appears to be essential in characterizing the lattice dynamics and, more importantly, its potential interaction with

†Corresponding author. E-mail: pjsun@iphy.ac.cn

© 2022 Chinese Physical Society and IOP Publishing Ltd

Dirac electrons.

2. Experimental methods

Single crystals of Cd_3As_2 were prepared by self-transport technique; see Ref. [5] for the details of structural characterization and crystal orientation. The specific heat was measured by thermal relaxation method in a commercial physical properties measurement system (PPMS, Quantum Design), and the thermal conductivity by conventional steady-state method with two thermometers and one heater.[5] The measurements of thermal expansion were performed by using a miniaturized capacitance dilatometer and an Andeen-Hagerling 2500A capacitance bridge.[17] We have also measured the transverse and longitudinal ultrasound velocities υ_T and υ_L of a large polycrystalline sample ($2.67 \times 1.97 \times 0.96$ mm^3). Here, the sound velocities were measured by a phase comparison technique,[18] where the frequency of the input acoustic wave was continuously adjusted during the temperature scan in order to maintain a constant phase of a given output echo. The elastic moduli were calculated from the ultrasound velocities as $C_i = d\upsilon_i^2$ ($i =$ L or T), with d being the sample density.

3. Results and discussion

The thermal conductivity $\kappa(T)$ measured within the as-grown (112) plane of a single crystal is shown in Fig. 1. Thermal measurements in the (100) plane have revealed very similar data,[8] indicating weak anisotropy of the thermal conductivity in Cd_3As_2. The electronic contribution $\kappa_e(T)$ calculated based on the Wiedemann–Franz law and the measured electrical resistivity (Fig. 1 inset) are also shown. In estimating the electronic part, we assume that the Sommerfeld value of the Lorenz number applies to this material in the temperature window of interest. We note, however, that to what extent the Wiedemann–Franz law holds in Dirac materials remains an issue of debate. For example, the Sommerfeld value of the Lorenz number may change significantly when a magnetic field is applied[19] or the Fermi level crosses the Dirac point;[20] the two situations that do not apply to the current work and Cd_3As_2. In spite of a moderate sample dependence of the $\kappa(T)$ profiles reported in the literature,[7,8,21] they are qualitatively similar with two marked features: a nearly temperature-independent, small value of $\kappa(T)$ at $T > 100$ K and a marked $\kappa(T)$ maximum at $T \approx 10$ K. The lattice thermal conductivity ($\kappa_L \approx \kappa - \kappa_e$) at $T > 100$ K falls into the range of the uncertainties (± 0.6 W/mK at room temperature) in our measurements, whereas the average κ_L reported in Ref. [8] is only 0.7 W/mK in the wide temperature range of 100−300 K. The small value of $\kappa_L(T)$ and its weak temperature dependence at $T > 100$ K indicate that the phonon mean free path is probably reduced to about its lower limit in this temperature range, in the framework of the simple kinetic approach, $\kappa_L = \frac{1}{3} C_L \bar{\upsilon} l$. Here, C_L is the lattice contribution to the specific heat, which tends to be constant at $T > 100$ K as determined by the Dulong–Petit limit (see Fig. 2 inset). The average phonon velocity ($\bar{\upsilon}$) can be estimated from our ultrasound measurements and is only weakly temperature dependent (within 5% in the whole temperature range investigated, see below).

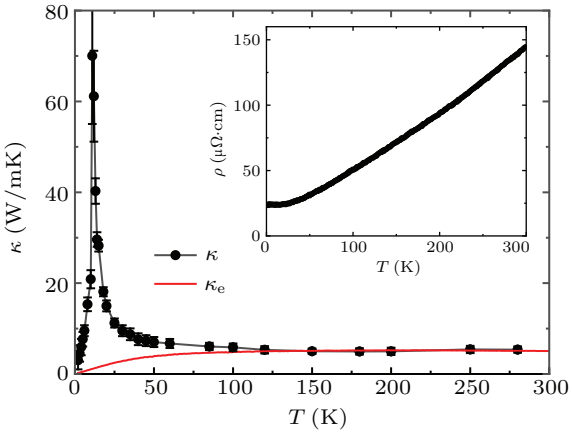


Fig. 1. The thermal conductivity $\kappa(T)$ measured within the as-grown (112) plane of Cd_3As_2. Error bars denote standard deviations estimated from the average of measurements under multiple temperature gradients. The electronic contribution $\kappa_e(T)$ (red solid line) is estimated from the Wiedemann–Franz law, $\kappa_e \rho / T = L_0$, with the Sommerfeld value of the Lorenz number $L_0 \equiv \frac{\pi^2}{3}(\frac{k_B}{2})^2 = 2.44 \times 10^{-8}$ W·Ω·K^{-2}.

Considering a reasonable value of $\kappa_L \approx 0.7$ W/mK for $T > 100$ K (Ref. [8]), the phonon mean free path l is estimated to be 6.96 Å, which is even shorter than the lattice parameters of Cd_3As_2, i.e., $a = b = 12.67$ Å and $c = 25.35$ Å. Note that, this is only a naive and rough estimate because on one hand the kinetic description of thermal conductivity is likely on the brink of failure for Cd_3As_2 with a large primitive cell,[22] and on the other hand the real phonon mean free path is actually mode dependent. Nevertheless, such estimate is meaningful because it confirms that the lattice thermal conductivity is already at or not far from its lower limit. The pronounced increase of $\kappa(T)$ below 50 K is a typical feature originated from phonon–phonon Umklapp processes, and the drastic decrease below about 10 K can be attributed to boundary scatterings of heat-carrying phonons in semimetals and semiconductors.[23] Here, the temperature-dependent specific heat determines the temperature profile of $\kappa(T)$ because the phonon mean free path is a constant. Though how the Dirac electrons impact on κ_L cannot be straightforwardly observed, it can be reliably inferred from κ_L as a function of the field: while κ_L is vanishingly small in zero and small fields ($B < 2$ T) where Dirac electrons are highly mobile, it increases gradually and becomes dominant in higher fields where Dirac electrons are spatially constrained by the magnetic fields; see $\kappa(B)$ shown in Fig. 2(e) of Ref. [5].

Before proceeding with other experimental results, we stress that a simple inspection into the crystal structure of

Cd_3As_2 can already yield important insight into the unusually low κ_L values. Cd_3As_2 crystallizes in a large primitive cell with the number of formula unit $Z = 16$, i.e., totally $N = 80$ atoms in one primitive cell. A large primitive cell means that the reciprocal space is predominantly occupied by a large number $(3N-3)$ of optical modes. As a result, the thermodynamically-weighted heat capacity and the Debye temperature for heat-carrying acoustic phonons are greatly suppressed. This causes a reduced κ_L from purely crystallographic reasons, as can be inferred from the aforementioned kinetic description for thermal conductivity. Such a strong reduction trend of κ_L with increasing primitive cell volume has been already reported previously.[24]

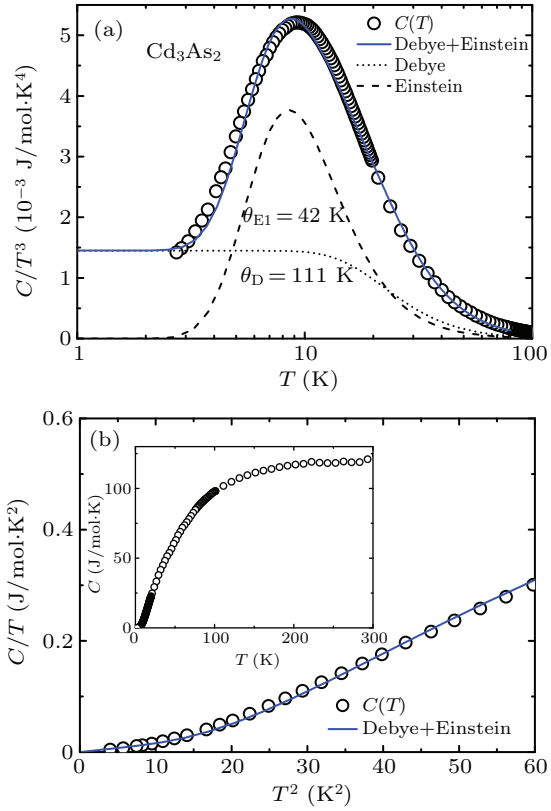


Fig. 2. (a) The low-temperature specific heat of Cd_3As_2 depicted as C/T^3 vs T. The data is fitted by considering a Debye term and two Einstein modes (blue solid line). Dotted and dashed lines are individual contributions from the Debye term and the leading Einstein mode, respectively (see text). (b) The low-temperature $C(T)$ deviates strongly from Debye's T-cube law that is commonly described by a linear dependence of C/T versus T^2. By contrast, the description based on the combined Debye and Einstein terms (blue solid line) can reasonably reproduce the curved $C/T(T^2)$ line. Inset: T-dependent specific heat of Cd_3As_2.

With the unusual thermal conductivity in mind, below we examine the specific heat carefully. Figure 2(a) displays the low-temperature specific heat as C/T^3 versus T. While the specific heat within Debye's description will obey a T-cube law and appear constant in this representation, an enhanced and broad peak is observed for Cd_3As_2 at $T \approx 10$ K. This is a thermodynamic signature of dominant low-energy optical modes, and has been intensively studied for cage compounds with "rattling" guest ion.[25] According to a rule of thumb obtained previously, the Einstein temperature θ_E characterizing these modes is five times the temperature position of the C/T^3 vs. T maximum, which means $\theta_E \approx 50$ K in this case.

The specific heat shown as C/T versus T^2 for $T < 8$ K in Fig. 2(b) further demonstrates the importance of low-energy Einstein modes. Different to the expectation from Debye's description, the $C/T(T^2)$ variation deviates significantly from a straight line. A linear dependence of $C/T(T^2)$, if any, appears only at $T^2 < 5$, namely, below about 2 K, where the contribution of low-energy optical models freezes out. Considering the significant contribution from soft optical phonons in the temperature window of interest, we combine Debye's description and a couple of local Einstein modes to fit $C(T)$,

$$C = (N_0 - \sum_n A_n) 9R \left(\frac{T}{\theta_D}\right)^3 \int_0^{\frac{\theta_D}{T}} \frac{\varepsilon^4 e^{\xi}}{(e^{\xi}-1)^2} d\xi + \sum_n (3RA_n \left(\frac{\theta_{En}}{T}\right)^2 \frac{e^{\frac{\theta_{En}}{T}}}{(e^{\frac{\theta_{En}}{T}}-1)^2}). \quad (1)$$

Here R is the gas constant, and A_n is the number of Einstein oscillations and N_0 is the number of atoms per formula unit. The result of fitting is shown by the blue solid line in Figs. 2(a) and 2(b), from which we obtain $\theta_D = 111$ K and $\theta_{E1} = 42$ K. A second Einstein mode with $\theta_{E2} = 101$ K, which is less important compared to the first one, was also included for a better fitting. Markedly, the fit can capture the prominent features in specific heat including the broad peak in C/T^3 versus T (Fig. 2(a)) and the curved C/T versus T^2 at low temperatures (Fig. 2(b)).

After confirmation of the existence of soft optical modes, we turn to examine the thermodynamics of acoustic modes. For this purpose, we have measured the longitudinal and transverse elastic moduli of a polycrystalline sample. The polycrystalline sample was prepared by grinding the single crystals into fine powder and pressing the powder into a small pellet. Compared to the single crystals, it is much larger and regular in shape, making it easy to accurately measure the absolute sound velocities and bulk modulus. In this case, only two independent and symmetry-averaged elastic moduli (C_L and C_T) exist, in stead of six independent elastic modes in single-crystalline sample Cd_3As_2. Figure 3 shows the elastic moduli $C_L(T)$ and $C_T(T)$ and their corresponding sound velocities that were directly measured, as well as the values of bulk modulus calculated as $K = C_L - \frac{4}{3}C_T$. The bulk modulus $K \approx 57.8$ GPa at 200 K is very close to that ($K = 54$ GPa) estimated from the lattice constants as a function of pressure.[14] Both $C_L(T)$ and $C_T(T)$ reveal no apparent anomaly and are characterized by smooth hardening upon cooling, as expected for typical solids. Nevertheless, we'd like to point out a weak feature that may be relevant to the Dirac states, i.e., an apparently damped harden-

ing of $C_T(T)$ at $T < 100$ K. That is, $C_T(T)$ tends to level off below 100 K and this behavior is almost absent in $C_L(T)$.

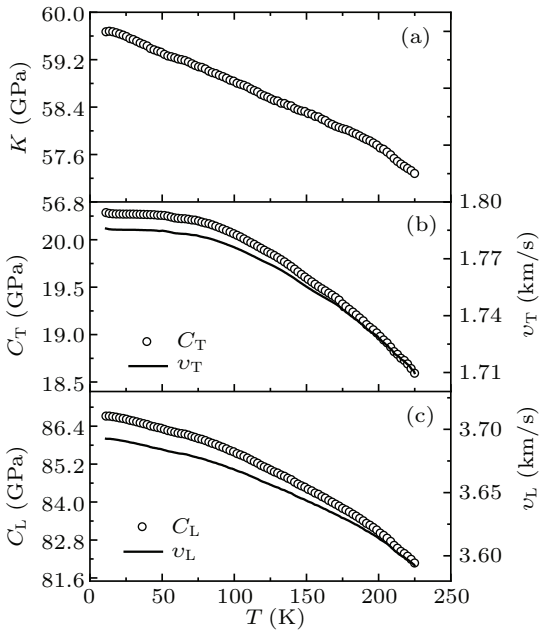


Fig. 3. Longitudinal (C_L) and transverse (C_T) elastic moduli and the calculated bulk modulus $K = C_L - \frac{4}{3}C_T$ as a function of temperature for Cd_3As_2. The corresponding longitudinal (υ_L) and transverse (υ_T) sound velocities are also shown (right axis).

From the longitudinal and transverse sound velocities of Cd_3As_2, the average sound velocity $\bar{\upsilon}$ can be calculated as follows:

$$\frac{1}{\bar{\upsilon}^3} = \frac{1}{3}\left(\frac{1}{\upsilon_L^3} + \frac{2}{\upsilon_T^3}\right). \tag{2}$$

From Eq. (2), one readily obtains $\bar{\upsilon} = 1943$ m/s for 200 K and 2005 m/s for 10 K. The moderately small sound velocities, which measure the phonon dispersions at the Brillouin zone center, are not the leading reason of the extremely low thermal conductivity. For comparison, $FeSb_2$, which has an average sound velocity of 3110 m/s (less than double $\bar{\upsilon}$ of Cd_3As_2) reveals a lattice thermal conductivity of several tens of W/mK at 100 K (Ref. [26]). Furthermore, the Debye temperature θ_D can also be estimated from the average phonon velocity

$$\theta_D = \frac{h\bar{\upsilon}}{k_B 2\pi}\sqrt[3]{6\pi^2 N/V}. \tag{3}$$

Here V is the primitive cell volume and h the Planck's constant. The estimated Debye temperature, $\theta_D = 187$ K, is considerably larger than that evaluated from the specific heat, $\theta_D = 111$ K. Unlike the specific heat which measures the thermodynamics of all low-energy phonons via the phonon density of states, sound velocities probe the group velocities of acoustic phonons at the low frequency limit and are less influenced by low-energy optical modes. The strong disagreement between the two values of θ_D hints at a strong deviation of the low-energy phonons from Debye's description, again pointing to the importance of low-energy optical modes in the description of the thermodynamic properties.

Figure 4 shows the linear thermal expansion coefficient estimated from the measured length change dL, $\alpha = 1/L(dL/dT)$, as a function of temperature. Here, α is measured along c axis of single-crystalline Cd_3As_2, which is the direction where Dirac cones are located.[10] In general, $\alpha(T)$ behaves similar to $C(T)$ (Fig. 2 inset); it reveals, however, negative values below about 10 K. Given the experimental results $K(T)$, $C(T)$ and $\alpha(T)$, one can easily estimate the Grüneisen ratio $\gamma = 3V_m K\alpha/C$ as an experimental indicator of lattice anharmonicity, where V_m is the molar volume.

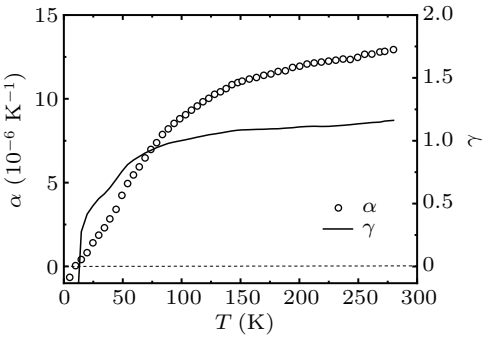


Fig. 4. Thermal expansion coefficient α measured along c axis (left) and the estimated thermodynamic Grüneisen ratio γ (right). Drastic drop of γ is observed at $T < 100$ K, ending up with negative values at $T < 10$ K.

As shown in Fig. 4 (right axis), $\gamma(T)$ remains 1.1 ($\pm$0.1) in a wide temperature range above 100 K. This is a Grüneisen ratio within the range of common expectation for simple solids. At $T < 100$ K, $\gamma(T)$ reveals a drastic drop and becomes negative at $T < 10$ K, corresponding to the low-temperature negative thermal expansion. The temperature window where $\gamma(T)$ drops significantly matches well to that where Einstein modes are observed in specific heat (Fig. 2). Phenomenologically, the unusual behavior of $\gamma(T)$ originates from the temperature dependence of $\alpha(T)$ that shows stronger decrease below 100 K relative to that of $C(T)$ towards negative values at low temperatures. Likewise, at $T \sim 100$ K, strong frequency reduction of several optical phonons has been observed by Raman scattering,[12] and this temperature has been regarded as a characteristic energy scale of interband scattering in the Dirac states coupling to low-energy optical phonons. In line with the negative values of $\gamma(T)$ that indicate lattice instability at low temperatures, the tetragonal metallic phase of Cd_3As_2 is indeed rather unstable and changes to a semiconducting monoclinic phase at a critical pressure $p_c \approx 2.3$ GPa,[14,16] as has been mentioned above. Different from the general expectation that pressure drives an insulator or a semiconductor to a metallic phase due to band broadening, the opposite trend observed in Cd_3As_2 indicates that the Dirac bands might play an important role in the structural instability, as inferred from our thermal expansion measurements. Because apparent anomaly

is not observed in the elastic moduli, we speculate the unusual $\gamma(T)$ behavior at low temperatures to be related to thermodynamics of low-energy optical modes.

4. Summary

To summarize, we have studied the low-energy phonons of Cd_3As_2 by a comprehensive set of thermodynamic probes. As far as the extremely low lattice thermal conductivity is concerned, Cd_3As_2 appears to be unusual in the following aspects: 1) A large unit cell sets a strong constraint on the thermodynamics of low-energy phonons, leading to reduced specific heat and enhanced phonon scattering rate of acoustic phonons; 2) Soft optical phonons, which are partially related to the Kohn anomaly caused by Dirac bands, can be clearly captured by low-temperature specific heat revealing significant Einstein terms; 3) A drastic decrease of the thermodynamic Grüneisen ratio is observed below 100 K, where enhanced coupling between lattice and electronic degrees of freedom has been previously confirmed. The decrease ends up with a negative thermal expansion at low temperatures that is indicative of lattice instability. At last, we note that while it is safe to conclude that the Dirac electrons are relevant to the phonon softening and the lattice instability in Cd_3As_2, to what extent the interplay between lattice dynamics and Dirac electrons plays its role therein remains an interesting issue. Because very low thermal conductivities have been observed in a number of topological semimetals such as $ZrTe_5$ (Ref. [27]), further investigation and comparison between different compounds along this line appear to be an interesting project.

Acknowledgements

This work was supported by the National Natural Science Foundation of China (Grant Nos. 11974389, 12141002 and 52088101), the National Key R&D Program of China (Grant No. 2017YFA0303100), the Chinese Academy of Sciences through the Scientific Instrument Developing Project (Grant No. ZDKYYQ20210003), and the Strategic Priority Research Program (Grant No. XDB33000000).

References

[1] Song Z D, Zhao J M, Fang Z and Dai X 2016 *Phys. Rev. B* **94** 214306
[2] Nguyen T, Han F, Andrejevic N, Pablo-Pedro R, Apte A, Tsurimaki Y, Ding Z W, Zhang K Y, Alatas A, Alp E E, Chi S X, Fernandez-Baca J, Matsuda M, Tennant D A, Zhao Y, Xu Z J, Lynn J W, Huang S X and Li M D 2020 *Phys. Rev. Lett.* **124** 236401
[3] Singh S, Wu Q S, Yue C M, Romero A H and Soluyanov A A 2018 *Phys. Rev. Mater.* **2** 114204
[4] Wang Z J, Weng H M, Wu Q S, Dai X and Fang Z 2013 *Phys. Rev. B* **88** 125427
[5] Xiang J S, Hu S L, Lyu M, Zhu W L, Ma C Y, Chen Z Y, Steglich F, Chen G F and Sun P J 2020 *Sci. China-Phys. Mech. Astron.* **63** 237011
[6] Spitzer D P, Castellion G A and Haacke G 1966 *J. Appl. Phys.* **37** 3795
[7] Zhang C, Zhou T, Liang S H, Cao J Z, Yuan X, Liu Y W, Shen Y, Wang Q S, Zhao J, Yang Z Q and Xiu F X 2016 *Chin. Phys. B* **25** 017202
[8] Wang H H, Luo X G, Chen W W, Wang N Z, Lei B, Meng F B, Shang C, Ma L K, Wu T, Dai X, Wang Z F and Chen X H 2018 *Sci. Bull.* **63** 411
[9] Toberer E S, Zevalkink A and Snyder G J 2011 *J. Mater. Chem.* **21** 15843
[10] Yue S Y, Chorsi H T, Goyal M, Schumann T, Yang R Q, Xu T S, Deng B W, Stemmer S, Schuller J A and Liao B L 2019 *Phys. Rev. Res.* **1** 033101
[11] Yue S Y, Deng B W, Liu Y M, Quan Y J, Yang R Q and Liao B L 2020 *Phys. Rev. B* **102** 235428
[12] Sharafeev A, Gnezdilov V, Sankar R, Chou F C and Lemmens P 2017 *Phys. Rev. B* **95** 235148
[13] Pietraszko A and Lukaszewicz K 1973 *Phys. Status Solidi A* **18** 723
[14] Gamża M, Abrami P, Gammond L V D, Ayres J, Osmond I, Muramatsu T, Armstrong R, Perryman H, Daisenberger D, Das S and Friedemann S 2021 *Phys. Rev. Mater.* **5** 024209
[15] Gupta S N, Muthu D V S, Shekhar C, Sankar R, Felser C and Sood A K 2017 *Europhys. Lett.* **120** 57003
[16] Zhang S, Wu Q, Schoop L, Ali M N, Shi Y G, Ni N, Gibson Q, Jiang S, Sidorov V, Yi W, Guo J, Zhou Y Z, Wu D S, Gao P W, Gu D C, Zhang C, Jiang S, Yang K, Li A G, Li Y C, Li X D, Liu J, Dai X, Fang Z, Cava R J, Sun L L and Zhao Z X 2015 *Phys. Rev. B* **91** 165133
[17] Küchler R, Bauer T, Brando M and Steglich F 2012 *Rev. Sci. Instru.* **83** 095102
[18] Lüthi B 2005 *Physical Acoustics in the Solid State* (Berlin: Springer-Verlag)
[19] Sharma G, Goswami P and Tewari S 2016 *Phys. Rev. B* **93** 035116
[20] Zhou H, Cai Y, Zhang G and Zhang Y W 2016 *Phys. Rev. B* **94** 045423
[21] Bartkowski K, Rafalowicz J and Zdanowicz W 1986 *Int. J. Thermophys.* **7** 765
[22] Simoncelli M, Marzari N and Mauri F 2019 *Nat. Phys.* **15** 809
[23] Tritt T 2004 *Thermal conductivity: theory, properties and applications* (New York: Kluwer Academic)
[24] Chen Z W, Zhang X Y and Pei Y Z 2018 *Adv. Mater.* **30** 1705617
[25] Matsuhira K, Sekine C, Wakeshima M, Hinatsu Y, Namiki T, Takeda K, Shirotani I, Sugawara H, Kikuchi D and Sato H 2009 *J. Phys. Soc. Jpn.* **78** 124601
[26] Bentien A, Johnsen S, Madsen G K H, Iversen B B and Steglich F 2007 *EPL* **80** 17008
[27] Zhu J, Feng T L, Mills S, Wang P P, Wu X W, Zhang L Y, Pantelides S T, Du X and Wang X J 2018 *ACS Appl. Mater. Interfaces* **10** 40740